Research Article Open Access

M. Cinefra*, S. Valvano, and E. Carrera

Heat conduction and Thermal Stress Analysis of laminated composites by a variable kinematic MITC9 shell element

DOI 10.1515/cls-2015-0017
Received March 23, 2015; accepted May 5, 2015

Abstract: The present paper considers the linear static thermal stress analysis of composite structures by means of a shell finite element with variable through-the-thickness kinematic. The temperature profile along the thickness direction is calculated by solving the Fourier heat conduction equation. The refined models considered are both Equivalent Single Layer (ESL) and Layer Wise (LW) and are grouped in the Unified Formulation by Carrera (CUF). These permit the distribution of displacements, stresses along the thickness of the multilayered shell to be accurately described. The shell element has nine nodes, and the Mixed Interpolation of Tensorial Components (MITC) method is used to contrast the membrane and shear locking phenomenon. The governing equations are derived from the Principle of Virtual Displacement (PVD). Cross-ply plate, cylindrical and spherical shells with simply-supported edges and subjected to bi-sinusoidal thermal load are analyzed. Various thickness ratios and curvature ratios are considered. The results, obtained with different theories contained in the CUF, are compared with both the elasticity solutions given in the literature and the analytical solutions obtained using the CUF and the Navier's method. Finally, plates and shells with different lamination and boundary conditions are analyzed using high-order theories in order to provide FEM benchmark solutions.

Keywords: Fourier heat conduction equation, Calculated Thermal Profile, Thermal stress analysis, Finite Element Method, Mixed Interpolated Tensorial Components, Carrera's Unified Formulation, Shell

***Corresponding Author: M. Cinefra:** Department of Aeronautics and Space Engineering, Politecnico di Torino, Corso Duca degli Abruzzi, 24, 10129 Turin, Italy, E-mail: maria.cinefra@polito.it, tel +39.011.546.6869, fax +39.011.564.6899
S. Valvano, E. Carrera: Department of Aeronautics and Space Engineering, Politecnico di Torino, Corso Duca degli Abruzzi, 24, 10129 Turin, Italy

1 Introduction

In the typical aeronautical structures composite materials have found an increasing amount of applications. Advanced composite materials combine a number of properties, including high specific strength and stiffness, and nearly zero coefficient of thermal expansion in the fiber orientation. These relevant properties result in a growing use of composite materials in structures subjected to severe thermal environment, such as high temperatures, high gradients and cycling changes of temperature. Consequently the thermal deformations and stresses which are induced by non-uniform temperature in composite structures become important parameters in structural design. Use of higher-order theories will make it possible to determine these parameters precisely in composite structures. In each developed computational model, the stress analysis should be preceded by an accurate thermal analysis, which provides the temperature input data required for the thermal external load. A satisfactory thermal stress analysis is only possible if advanced and refined computational models are developed to correctly approximate the stiffness matrix, and if a correct thermal load is recognized. Sometimes the evaluation of a correct thermal load could be mandatory with respect to any further evaluation for the computational models.

Studies involving the thermo-elastic behaviour using classical or first-order theories are described by Kant and Khare [1] and Khdeir and Reddy [2]. In recent years, several higher-order two-dimensional models have been developed for such problems, which consider only an assumed temperature profile through the thickness. Among these, of particular interest is the higher-order model by Whu and Chen [3]. The same temperature profile is used by Khare et alii [4] to obtain a closed-form solution for the thermomechanical analysis of laminated and sandwich shells. Khdeir [5] and Khdeir et alii [6] assume a linear or constant temperature profile through the thickness. Barut et alii [7] analyze the non-linear thermoelastic behavior of shells by means of the Finite Element Method, but the assigned temperature profile is linear. In the framework

of the arbitrary distribution of temperature through the thickness, Miller et alii [8] and Dumir et alii [9] are noteworthy, in the first a classical shell theory for composite shells is given, the second remarks the importance of the zig-zag form of displacements in the thermal analysis of composite shells. In the case of shells, further investigations were made by Hsu et alii [10] for both closed form and Finite Element method, and by Ding [11] for a weak formulation for the case of state equations including the boundary conditions.

In the last few years many contributions have been proposed, which are based on Carrera Unified Formulation, to investigate the thermal effects in composite structures. In [12] a study on the influence of the through-the-thickness temperature profile on the thermo-mechanical response of multilayered anisotropic thick and thin plates has been addressed. The partially coupled stress problem was considered by solving the Fourier's conductivity equation. The importance of mixed theories for a correct prediction of transverse shear/normal stresses due to thermal loadings have been remarked in [13, 14]. A fully coupled thermo-mechanical analysis applied to plate structure is employed in [15]. Different type of loads as problems related to uniform, triangular, bi-triangular (tentlike), and localized in-plane distribution of temperature were considered in [16]. The Ritz method, based on the choice of trigonometric trial functions, was used in [17]. Extension to Functionally Graded Materials (FGMs) has been done in [18]. A thermal stability analysis of functionally graded material, isotropic and sandwich plates is studied in [19], the Ritz method is employed and uniform, linear, and non-linear temperature profile is taken into account for different cases. An extension of the thermoelastic formulation to shells has been done in [20] and the Fourier heat conduction equation was employed for shell in [21]. The thermo-mechanical analysis of functionally graded shell is considered in [22]. Analytical closed form solutions are available in very few cases. The solution of the most of the practical problems demand applications of approximated computational methods.

In this paper, the authors desire to demonstrate as the assumption of a priori linear temperature profile in the thickness direction could be wrong for particular shell and plate configurations, and as the use of the Fourier heat conduction equation could result mandatory to obtain a correct thermal load. Therefore, we would like to demonstrate as a wrong thermal load invalidates the static response of plate and shell structures even when advanced computational models are employed. An improved doubly-curved shell finite element for the analysis of composite structures under thermal loads is here presented, it is a natural extension of the plate finite element presented in [23]. The shell finite element is based on the Carrera's Unified Formulation (CUF), which was developed by Carrera for multi-layered structures [24, 25]. Both Equivalent Single Layer (ESL) and Layer Wise (LW) theories contained in the CUF have been implemented in the shell finite element. The Mixed Interpolation of Tensorial Components (MITC) method [26–29] is used to contrast the membrane and shear locking. The governing equations for the linear static analysis of composite structures are derived from the Principle of Virtual Displacement (PVD), in order to apply the finite element method. The temperature profile is calculated solving the Fourier heat conduction equation and compared with the linear profile through the thickness for each two-dimensional model. Cross-ply plate, cylindrical and spherical shells with simply-supported edges and subjected to bi-sinusoidal thermal loads are analyzed. The results obtained with the different models contained in the CUF, are compared with the exact solution given in the literature and the analytical Navier's solution type. Finally, plates and shells with different lamination and boundary conditions are also analyzed using high-order theories in order to provide FEM benchmark solutions

2 Geometrical and constitutive relations for shell

Shells are bi-dimensional structures in which one dimension (in general the thickness in z direction) is negligible with respect to the other two in-plane dimensions. Geometry and the reference system are indicated in Fig. 1. By considering multilayered structures, the square of an infinitesimal linear segment in the layer, the associated infinitesimal area and volume are given by:

$$\begin{aligned} ds_k^2 &= H_\alpha^{k\,2}\, d\alpha_k^2 + H_\beta^{k\,2}\, d\beta_k^2 + H_z^{k\,2}\, dz_k^2 \,, \\ d\Omega_k &= H_\alpha^k H_\beta^k\, d\alpha_k\, d\beta_k \,, \\ dV &= H_\alpha^k\, H_\beta^k\, H_z^k\, d\alpha_k\, d\beta_k\, dz_k \,, \end{aligned} \tag{1}$$

where the metric coefficients are:

$$H_\alpha^k = A^k(1 + z_k/R_\alpha^k), \quad H_\beta^k = B^k(1 + z_k/R_\beta^k), \quad H_z^k = 1 \,. \tag{2}$$

k denotes the k-layer of the multilayered shell; R_α^k and R_β^k are the principal radii of the midsurface of the layer k. A^k and B^k are the coefficients of the first fundamental form of

Ω_k (Γ_k is the Ω_k boundary). In this paper, the attention has been restricted to shells with constant radii of curvature (cylindrical, spherical, toroidal geometries) for which $A^k = B^k = 1$. Details for shells are reported in [30].

Geometrical relations permit the in-plane $\boldsymbol{\epsilon}_p^k$ and out-plane $\boldsymbol{\epsilon}_n^k$ strains to be expressed in terms of the displacement $\boldsymbol{u}$. The following relations hold:

$$\begin{aligned}\boldsymbol{\epsilon}_p^k &= [\epsilon_{\alpha\alpha}^k, \epsilon_{\beta\beta}^k, \epsilon_{\alpha\beta}^k]^T = (\boldsymbol{D}_p^k + \boldsymbol{A}_p^k)\,\boldsymbol{u}^k\,,\\ \boldsymbol{\epsilon}_n^k &= [\epsilon_{\alpha z}^k, \epsilon_{\beta z}^k, \epsilon_{zz}^k]^T = (\boldsymbol{D}_{n\Omega}^k + \boldsymbol{D}_{nz}^k - \boldsymbol{A}_n^k)\,\boldsymbol{u}^k\,.\end{aligned} \tag{3}$$

The explicit form of the introduced arrays is:

$$\boldsymbol{D}_p^k = \begin{bmatrix} \frac{\partial_\alpha}{H_\alpha^k} & 0 & 0 \\ 0 & \frac{\partial_\beta}{H_\beta^k} & 0 \\ \frac{\partial_\beta}{H_\beta^k} & \frac{\partial_\alpha}{H_\alpha^k} & 0 \end{bmatrix}, \quad \boldsymbol{D}_{n\Omega}^k = \begin{bmatrix} 0 & 0 & \frac{\partial_\alpha}{H_\alpha^k} \\ 0 & 0 & \frac{\partial_\beta}{H_\beta^k} \\ 0 & 0 & 0 \end{bmatrix},$$

$$\boldsymbol{D}_{nz}^k = \begin{bmatrix} \partial_z & 0 & 0 \\ 0 & \partial_z & 0 \\ 0 & 0 & \partial_z \end{bmatrix}, \tag{4}$$

$$\boldsymbol{A}_p^k = \begin{bmatrix} 0 & 0 & \frac{1}{H_\alpha^k R_\alpha^k} \\ 0 & 0 & \frac{1}{H_\beta^k R_\beta^k} \\ 0 & 0 & 0 \end{bmatrix}, \; \boldsymbol{A}_n^k = \begin{bmatrix} \frac{1}{H_\alpha^k R_\alpha^k} & 0 & 0 \\ 0 & \frac{1}{H_\beta^k R_\beta^k} & 0 \\ 0 & 0 & 0 \end{bmatrix}. \tag{5}$$

The definition of the 3D constitutive equations permits the stresses to be expressed by means of the strains. The generalized Hooke's law is considered, by employing a linear constitutive model for infinitesimal deformations. In a composite material, these equations are obtained in material coordinates (1, 2, 3) for each orthotropic layer k and then rotated in the general curvilinear reference system (α, β, z). Therefore, the stress-strain relations after the rotation are:

$$\begin{aligned}\boldsymbol{\sigma}_p^k &= [\sigma_{\alpha\alpha}^k, \sigma_{\beta\beta}^k, \sigma_{\alpha\beta}^k]^T = \boldsymbol{\sigma}_{pd}^k - \boldsymbol{\sigma}_{pT}^k = \boldsymbol{C}_{pp}^k\,\boldsymbol{\epsilon}_p^k + \boldsymbol{C}_{pn}^k\,\boldsymbol{\epsilon}_n^k - \boldsymbol{\lambda}_p^k\,\theta^k\\ \boldsymbol{\sigma}_n^k &= [\sigma_{\alpha z}^k, \sigma_{\beta z}^k, \sigma_{zz}^k]^T = \boldsymbol{\sigma}_{nd}^k - \boldsymbol{\sigma}_{nT}^k = \boldsymbol{C}_{np}^k\,\boldsymbol{\epsilon}_p^k + \boldsymbol{C}_{nn}^k\,\boldsymbol{\epsilon}_n^k - \boldsymbol{\lambda}_n^k\,\theta^k\end{aligned} \tag{6}$$

where

$$\boldsymbol{C}_{pp}^k = \begin{bmatrix} C_{11}^k & C_{12}^k & C_{16}^k \\ C_{12}^k & C_{22}^k & C_{26}^k \\ C_{16}^k & C_{26}^k & C_{66}^k \end{bmatrix} \quad \boldsymbol{C}_{pn}^k = \begin{bmatrix} 0 & 0 & C_{13}^k \\ 0 & 0 & C_{23}^k \\ 0 & 0 & C_{36}^k \end{bmatrix}$$

$$\boldsymbol{C}_{np}^k = \begin{bmatrix} 0 & 0 & 0 \\ 0 & 0 & 0 \\ C_{13}^k & C_{23}^k & C_{36}^k \end{bmatrix} \quad \boldsymbol{C}_{nn}^k = \begin{bmatrix} C_{55}^k & C_{45}^k & 0 \\ C_{45}^k & C_{44}^k & 0 \\ 0 & 0 & C_{33}^k \end{bmatrix} \tag{7}$$

$$\begin{aligned}\boldsymbol{\lambda}_p^k &= \boldsymbol{C}_{pp}^k\,\boldsymbol{\alpha}_p^k + \boldsymbol{C}_{pn}^k\,\boldsymbol{\alpha}_n^k\\ \boldsymbol{\lambda}_n^k &= \boldsymbol{C}_{np}^k\,\boldsymbol{\alpha}_p^k + \boldsymbol{C}_{nn}^k\,\boldsymbol{\alpha}_n^k\end{aligned} \tag{8}$$

$$\boldsymbol{\alpha}_p^k = \begin{bmatrix} \boldsymbol{\alpha}_1^k \\ \boldsymbol{\alpha}_2^k \\ 0 \end{bmatrix} \qquad \boldsymbol{\alpha}_n^k = \begin{bmatrix} 0 \\ 0 \\ \boldsymbol{\alpha}_3^k \end{bmatrix} \tag{9}$$

$$\boldsymbol{\lambda}_p^k = \begin{bmatrix} \boldsymbol{\lambda}_1^k \\ \boldsymbol{\lambda}_2^k \\ \boldsymbol{\lambda}_6^k \end{bmatrix} \qquad \boldsymbol{\lambda}_n^k = \begin{bmatrix} 0 \\ 0 \\ \boldsymbol{\lambda}_3^k \end{bmatrix} \tag{10}$$

The subscripts d and T mean mechanical and thermal contributions. The material coefficients C_{ij} depend on the Young's moduli E_1, E_2, E_3, the shear moduli G_{12}, G_{13}, G_{23} and Poisson moduli $\nu_{12}, \nu_{13}, \nu_{23}, \nu_{21}, \nu_{31}, \nu_{32}$ that characterize the layer material. α_{ij} are the thermal expansion coefficients, λ_{ij} are the coefficients of thermo-mechanical coupling and θ^k is the difference with a reference temperature.

3 Carrera Unified Formulation for Shell

The variation of the displacement variables along the thickness direction is a-priori postulated. Several displacement-based theories can be formulated on the basis of the following generic kinematic field. The main feature of the Unified Formulation by Carrera [25, 31, 32] (CUF) is the unified manner in which the displacement variables are handled.

$$\begin{aligned}&\boldsymbol{u}^k(\alpha, \beta, z) = F_s(z)\boldsymbol{u}_s^k(\alpha, \beta);\\ &\delta\boldsymbol{u}^k(\alpha, \beta, z) = F_\tau(z)\delta\boldsymbol{u}_\tau^k(\alpha, \beta) \qquad \tau, s = 0, 1, \ldots, N\end{aligned} \tag{11}$$

where (α, β, z) is a curvilinear reference system, in which α and β are orthogonal and the curvature radii R_α and R_β are constant in each point of the domain Ω (see Fig. 1). The displacement vector $\boldsymbol{u} = \{u, v, w\}$ has its components expressed in this system. $\delta\boldsymbol{u}$ indicates the virtual displacement associated to the virtual work and k identifies the layer. F_τ and F_s are the so-called thickness functions depending only on z. $\boldsymbol{u}_s$ are the unknown variables depending on the coordinates α and β. τ and s are sum indexes and N is the order of expansion in the thickness direction assumed for the displacements.

Classical Theories

The simplest plate/shell theory is based on the Kirchhoff/Love's hypothesis, and it is usually referred to as Classical Lamination Theory (CLT)[33],[34]. Both transverse

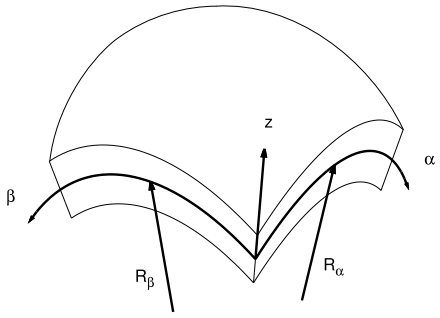

Figure 1: Reference system of the double curvature shell.

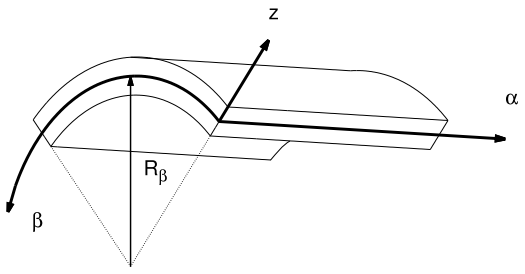

Figure 2: Reference system of the cylindrical shell.

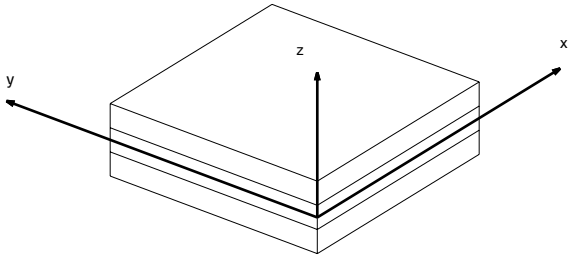

Figure 3: Reference system of the plate.

shear strains and transverse normal strains are discarded, in usual applications being negligible with respect to the in-plane ones,

$$\begin{cases} u(\alpha,\beta,z) = u_0(\alpha,\beta) - z\dfrac{\partial w_0}{\partial \alpha} \\ v(\alpha,\beta,z) = v_0(\alpha,\beta) - z\dfrac{\partial w_0}{\partial \beta} \\ w(\alpha,\beta,z) = w_0(\alpha,\beta) \end{cases} \tag{12}$$

The inclusion of transverse shear strains, in the theory mentioned here, leads to Reissner-Mindlin Theory, also known as First-order Shear Deformation Theory (FSDT) [35],

$$\begin{cases} u(\alpha,\beta,z) = u_0(\alpha,\beta) + z\,u_1(\alpha,\beta) \\ v(\alpha,\beta,z) = v_0(\alpha,\beta) + z\,v_1(\alpha,\beta) \\ w(\alpha,\beta,z) = w_0(\alpha,\beta) \end{cases} \tag{13}$$

However, these theories, due to their inconsistency in discarding the transverse normal stress in the material constitutive equations, are no longer valid when 3D local effects appear. Among these, stretching effects are neglected in CLT and FSDT models because the transverse displacement is assumed constant in the thickness direction. Moreover, local effects due to concentrated loads cannot be represented if linear displacement field is considered. To remove the inconsistency completely, higher-order expansion of the unknown with respect to the z coordinate are needed. For more details, the readers can refer to the article [24].

Equivalent Single Layer Theories

Many attempts have been made to improve classical plate/shell models. The CUF has the capability to expand each displacement variable in the displacement field at any desired order independently from the others and with respect to the accuracy and the computational cost has been introduced. Such an artifice permits us to treat each variable independently from the others. This becomes extremely useful when multifield problems are investigated such as thermoelastic and piezoelectric applications [13, 20, 36].

In the case of Equivalent Single Layer (ESL) models, a Taylor expansion is employed as thickness functions:

$$\boldsymbol{u} = F_0\boldsymbol{u}_0 + F_1\boldsymbol{u}_1 + \ldots + F_N\boldsymbol{u}_N = F_s\boldsymbol{u}_s, \qquad s = 0, 1, \ldots, N. \tag{14}$$

$$F_0 = z^0 = 1, \quad F_1 = z^1 = z, \quad \ldots, \quad F_N = z^N. \tag{15}$$

Following this approach the displacement field can be written as:

$$\begin{cases} u(\alpha,\beta,z) = u_0(\alpha,\beta) + z\,u_1(\alpha,\beta) + \ldots + z^N\,u_N(\alpha,\beta) \\ v(\alpha,\beta,z) = v_0(\alpha,\beta) + z\,v_1(\alpha,\beta) + \ldots + z^N\,v_N(\alpha,\beta) \\ w(\alpha,\beta,z) = w_0(\alpha,\beta) + z\,w_1(\alpha,\beta) + \ldots + z^N\,w_N(\alpha,\beta) \end{cases} \tag{16}$$

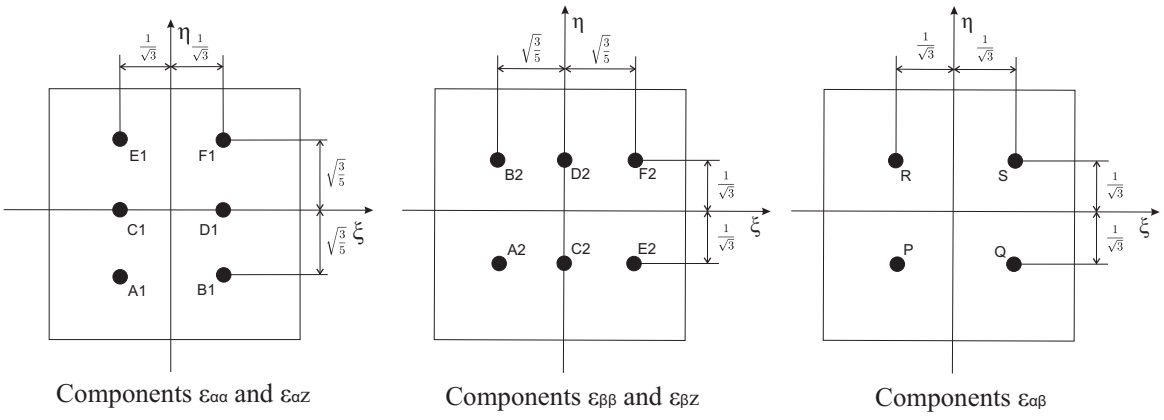

Figure 4: Tying points for the MITC9 shell finite element.

In general:

$$\begin{cases} u(\alpha,\beta,z) = F_0(\alpha,\beta) + F_1\, u_1(\alpha,\beta) + \ldots + F_N\, u_N(\alpha,\beta) \\ v(\alpha,\beta,z) = F_0(\alpha,\beta) + F_1\, v_1(\alpha,\beta) + \ldots + F_N\, v_N(\alpha,\beta) \\ w(\alpha,\beta,z) = F_0(\alpha,\beta) + F_1\, w_1(\alpha,\beta) + \ldots + F_N\, w_N(\alpha,\beta) \end{cases} \tag{17}$$

Classical models, such as those based on the First-order Shear Deformation Theory (FSDT), can be obtained from an ESL theory with $N = 1$, by imposing a constant transverse displacement through the thickness via penalty techniques (that is, the degree of freedom given by the linear part of the transverse displacement is penalized by assigning infinite value to the corresponding term in the diagonal of the stiffness matrix). Also a model based on the hypotheses of Classical Lamination Theory (CLT) can be expressed by means of the CUF by applying a penalty technique to the constitutive equations (the penalty is here applied to the shear modulus in the matrix of the material coefficients). This permits to impose null transverse shear strains in the shell.

Zig-Zag Models and Layer Wise Theories

Due to the intrinsic anisotropy of multilayered structures, the first derivative of the displacement variables in the z-direction is discontinuous. The Layer-Wise (LW) models, in respect to the ESLs, allow the zig-zag form of the displacement distribution in layered structures to be modelled. It is possible to reproduce the zig-zag effects also in the framework of the ESL description by employing the Murakami theory. According to references [37], a zig-zag term can be introduced into equation(14) as follows:

$$\boldsymbol{u}^k = F_0\, \boldsymbol{u}_0^k + \ldots + F_N\, \boldsymbol{u}_N^k + (-1)^k \zeta_k \boldsymbol{u}_Z^k. \tag{18}$$

Subscript Z refers to the introduced term. Such theories are called zig-zag (Z) theories. Following this approach the displacement field can be written as:

$$\begin{cases} u(\alpha,\beta,z) = F_0(\alpha,\beta) + F_1\, u_1(\alpha,\beta) + \ldots \\ \qquad +F_{N-1}\, u_{N-1}(\alpha,\beta) + (-1)^k \zeta_k u_{Z_N}^k \\ v(\alpha,\beta,z) = F_0(\alpha,\beta) + F_1\, v_1(\alpha,\beta) + \ldots \\ \qquad +F_{N-1}\, v_{N-1}(\alpha,\beta) + (-1)^k \zeta_k v_{Z_N}^k \\ w(\alpha,\beta,z) = F_0(\alpha,\beta) + F_1\, w_1(\alpha,\beta) + \ldots \\ \qquad +F_{N-1}\, w_{N-1}(\alpha,\beta) + (-1)^k \zeta_k w_{Z_N}^k \end{cases} \tag{19}$$

In the case of Layer-Wise (LW) models, the displacement is defined at k-layer level:

$$\boldsymbol{u}^k = F_t\, \boldsymbol{u}_t^k + F_b\, \boldsymbol{u}_b^k + F_r\, \boldsymbol{u}_r^k = F_s\, \boldsymbol{u}_s^k, \quad s = t, b, r, \quad r = 2, \ldots, N. \tag{20}$$

$$F_t = \frac{P_0 + P_1}{2}, \quad F_b = \frac{P_0 - P_1}{2}, \quad F_r = P_r - P_{r-2}. \tag{21}$$

in which $P_j = P_j(\zeta_k)$ is the Legendre polynomial of j-order defined in the ζ_k-domain: $-1 \le \zeta_k \le 1$. $P_0 = 1, P_1 = \zeta_k, P_2 = (3\zeta_k^2 - 1)/2, P_3 = (5\zeta_k^3 - 3\zeta_k)/2, P_4 = (35\zeta_k^4 - 30\zeta_k^2 + 3)/8$. The top ($t$) and bottom ($b$) values of the displacements are used as unknown variables and one can impose the following compatibility conditions:

$$u_t^k = u_b^{k+1}, \qquad k = 1, N_l - 1. \tag{22}$$

4 Finite Element approximation and MITC9 method

In this section, the derivation of a shell finite element for the analysis of multilayered structures is presented. The element is based on both the ESL and LW theories contained

in the Unified Formulation. After an overview in scientific literature about the methods that permit to withstand the membrane and shear locking, the MITC technique has been adopted for this element. Considering a 9-nodes finite element with doubly-curved geometry, the displacement components are interpolated on the nodes of the element by means of the Lagrangian shape functions N_i [38]:

$$\boldsymbol{u}_s = N_j \boldsymbol{u}_{s_j} \qquad \delta\boldsymbol{u}_\tau = N_i \delta\boldsymbol{u}_{\tau_i} \qquad \text{with} \quad i,j = 1,\ldots,9 \tag{23}$$

where $\boldsymbol{u}_{s_j}$ and $\delta\boldsymbol{u}_{\tau_i}$ are the nodal displacements and their virtual variations. Substituting in the geometrical relations (3) one has:

$$\begin{aligned} \boldsymbol{\epsilon}_p &= F_\tau(\boldsymbol{D}_p + \boldsymbol{A}_p)(N_i\boldsymbol{I})\boldsymbol{u}_{\tau_i} \\ \boldsymbol{\epsilon}_n &= F_\tau(\boldsymbol{D}_{n\Omega} - \boldsymbol{A}_n)(N_i\boldsymbol{I})\boldsymbol{u}_{\tau_i} + F_{\tau,z}(N_i\boldsymbol{I})\boldsymbol{u}_{\tau_i} \end{aligned} \tag{24}$$

where $\boldsymbol{I}$ is the identity matrix.

Considering the local coordinate system (ξ, η), the MITC shell elements ([39]-[40]) are formulated by using, instead of the strain components directly computed from the displacements, an interpolation of these within each element using a specific interpolation strategy for each component. The corresponding interpolation points, called *tying points*, are shown in Fig. 4 for a nine-nodes element. Note that the transverse normal strain ϵ_{zz} is excluded from this procedure and it is directly calculated from the displacements.

The interpolating functions are Lagrangian functions and are arranged in the following arrays:

$$\begin{aligned} N_{m1} &= [N_{A1}, N_{B1}, N_{C1}, N_{D1}, N_{E1}, N_{F1}] \\ N_{m2} &= [N_{A2}, N_{B2}, N_{C2}, N_{D2}, N_{E2}, N_{F2}] \\ N_{m3} &= [N_P, N_Q, N_R, N_S] \end{aligned} \tag{25}$$

From this point on, the subscripts $m1$, $m2$ and $m3$ indicate quantities calculated in the points $(A1, B1, C1, D1, E1, F1)$, $(A2, B2, C2, D2, E2, F2)$ and (P, Q, R, S), respectively. Therefore, the strain components are interpolated as follows:

$$\begin{aligned} \boldsymbol{\epsilon}_p &= \begin{bmatrix} \epsilon_{\alpha\alpha} \\ \epsilon_{\beta\beta} \\ \epsilon_{\alpha\beta} \end{bmatrix} = \begin{bmatrix} N_{m1} & 0 & 0 \\ 0 & N_{m2} & 0 \\ 0 & 0 & N_{m3} \end{bmatrix} \begin{bmatrix} \epsilon_{\alpha\alpha_{m1}} \\ \epsilon_{\beta\beta_{m2}} \\ \epsilon_{\alpha\beta_{m3}} \end{bmatrix} \\ \boldsymbol{\epsilon}_n &= \begin{bmatrix} \epsilon_{\alpha z} \\ \epsilon_{\beta z} \\ \epsilon_{zz} \end{bmatrix} = \begin{bmatrix} N_{m1} & 0 & 0 \\ 0 & N_{m2} & 0 \\ 0 & 0 & 1 \end{bmatrix} \begin{bmatrix} \epsilon_{\alpha z_{m1}} \\ \epsilon_{\beta z_{m2}} \\ \epsilon_{zz} \end{bmatrix} \end{aligned} \tag{26}$$

where the strains $\epsilon_{\alpha\alpha_{m1}}$, $\epsilon_{\beta\beta_{m2}}$, $\epsilon_{\alpha\beta_{m3}}$, $\epsilon_{\alpha z_{m1}}$, $\epsilon_{\beta z_{m2}}$ are expressed by means of eq.s (24) in which the shape functions N_i and their derivatives are evaluated in the tying points. For example, one can considers the strain component $\epsilon_{\alpha\alpha}$ that is calculated as follows:

$$\begin{aligned} \epsilon_{\alpha\alpha} =& N_{A1}\epsilon_{\alpha\alpha_{A1}} + N_{B1}\epsilon_{\alpha\alpha_{B1}} + N_{C1}\epsilon_{\alpha\alpha_{C1}} + N_{D1}\epsilon_{\alpha\alpha_{D1}} \\ &+ N_{E1}\epsilon_{\alpha\alpha_{E1}} + N_{F1}\epsilon_{\alpha\alpha_{F1}} \end{aligned} \tag{27}$$

with:

$$\epsilon_{\alpha\alpha_{A1}} = N^{(A1)}_{i,\alpha} F_\tau u_{\tau_i} + \frac{1}{H_\alpha R_\alpha} N^{(A1)}_i F_\tau w_{\tau_i} \tag{28}$$

The superscript $(A1)$ indicates that the shape function and its derivative are evaluated in the point of coordinates $(-\frac{1}{\sqrt{3}}, -\sqrt{\frac{3}{5}})$. Similar expressions can be written for $\epsilon_{\alpha\alpha_{B1}}, \epsilon_{\alpha\alpha_{C1}}, \epsilon_{\alpha\alpha_{D1}}, \epsilon_{\alpha\alpha_{E1}}, \epsilon_{\alpha\alpha_{F1}}$.

5 Governing FEM equations

The PVD for a multilayered doubly-curved shell reads:

$$\int_{\Omega_k}\int_{A_k} \left\{ \delta{\boldsymbol{\epsilon}_p^k}^T \boldsymbol{\sigma}_p^k + \delta{\boldsymbol{\epsilon}_n^k}^T \boldsymbol{\sigma}_n^k \right\} H_\alpha^k H_\beta^k \, d\Omega_k dz = \delta L_e \tag{29}$$

where Ω_k and A_k are the integration domains in the plane and in the thickness direction, respectively. The left hand side of the equation represents the variation of the internal work, while the right hand side is the external work. $\boldsymbol{\sigma}_p^k$ and $\boldsymbol{\sigma}_n^k$ contain the mechanical (d) and thermal (T) contributions, so:

$$\begin{aligned} &\int_{\Omega_k}\int_{A_k} \left\{ \delta{\boldsymbol{\epsilon}_p^k}^T \left(\boldsymbol{\sigma}_{pd}^k - \boldsymbol{\sigma}_{pT}^k \right) + \delta{\boldsymbol{\epsilon}_n^k}^T \left(\boldsymbol{\sigma}_{nd}^k - \boldsymbol{\sigma}_{nT}^k \right) \right\} H_\alpha^k H_\beta^k \, d\Omega_k dz \\ &= \delta L_e \end{aligned} \tag{30}$$

In this work no mechanical loads are applied to the shell structure, so the external work is null, except for the thermal stress contribution of the temperature distribution applied, so:

$$\begin{aligned} &\int_{\Omega_k}\int_{A_k} \left\{ \delta{\boldsymbol{\epsilon}_p^k}^T \boldsymbol{\sigma}_{pd}^k + \delta{\boldsymbol{\epsilon}_n^k}^T \boldsymbol{\sigma}_{nd}^k \right\} H_\alpha^k H_\beta^k \, d\Omega_k dz \\ &= \int_{\Omega_k}\int_{A_k} \left\{ \delta{\boldsymbol{\epsilon}_p^k}^T \boldsymbol{\sigma}_{pT}^k + \delta{\boldsymbol{\epsilon}_n^k}^T \boldsymbol{\sigma}_{nT}^k \right\} H_\alpha^k H_\beta^k \, d\Omega_k dz \end{aligned} \tag{31}$$

Substituting the constitutive equations (6), the geometrical relations written via the MITC method (26) and applying the Unified Formulation (11) and the FEM approximation (23), one obtains the following governing equations:

$$\delta\boldsymbol{q}_u^{k\tau i} : \quad \boldsymbol{K}_{uu}^{k\tau sij} \boldsymbol{q}_u^{ksj} = \boldsymbol{\Theta}^{k\tau i} \tag{32}$$

where $\boldsymbol{K}_{uu}^{k\tau sij}$ is a 3 × 3 matrix, called fundamental nucleus of the mechanical stiffness matrix, and its explicit expression is given in [41]. This is the basic element from which the stiffness matrix of the whole structure is computed. The fundamental nucleus is expanded on the indexes τ and s in order to obtain the stiffness matrix of each layer. Then, the matrices of each layer are assembled at multilayer level depending on the approach considered, ESL or LW. $\boldsymbol{\Theta}^{k\tau i}$ is a 3 × 1 matrix, called fundamental nucleus of the thermal load, and its explicit expression is given in the following section. $\boldsymbol{q}_u^{ksj}$ and $\delta\boldsymbol{q}_u^{k\tau i}$ are the nodal displacements and their virtual variation, respectively.

6 Heat conduction problem in layered structures

The heat conduction problem is investigated by solving the Fourier heat conduction equation as described in [42] for the plate case. Here the solution is given for the shell case as proposed in [21]. If the values of the temperature are known at the top and bottom surface of the shell, the temperature profile through the thickness can be considered in two different ways. The first method introduces an assumed profile $\hat{\theta}(z)$ that varies linearly from the top to the bottom as follows:

$$\hat{\theta}(z) = \theta_{bottom} + \frac{\theta_{top} - \theta_{bottom}}{h} \star \left(z + \frac{h}{2}\right) \qquad z \in \left[\frac{-h}{2}\,;\,\frac{h}{2}\right] \tag{33}$$

Independently by the number of considered layers the linear profile is always the same.

The second one computes $\hat{\theta}(z)$ by solving the Fourier heat conduction equation. In case of multi-layered structures, in general for the k^{th} homogeneous orthotropic layer, the differential Fourier equation of heat conduction reads:

$$\left(\frac{K_1^k}{(H_\alpha^k)^2}\right)\frac{\delta^2\theta}{\delta\alpha^2} + \left(\frac{K_2^k}{(H_\beta^k)^2}\right)\frac{\delta^2\theta}{\delta\beta^2} + \left(K_3^k\right)\frac{\delta^2\theta}{\delta z^2} = 0 \tag{34}$$

where K_1^k, K_2^k, K_3^k are the thermal conductivities coefficients in material coordinates (1, 2, 3) for each orthotropic layer k and then rotated in the general curvilinear reference system (α, β, z). In case of multi-layered structures, continuity conditions for the temperature θ and the transverse normal heat flux q_z hold in the thickness direction at each k^{th} layer interface, reading:

$$\theta_t^k = \theta_b^{k+1} \qquad q_{zt}^k = q_{zb}^{k+1} \qquad for\, k = 1, \ldots, N_l - 1 \tag{35}$$

where N_l is the number of layers in the considered structure. The relationship between the transverse heat flux and the temperature is given as:

$$q_z^k = K_3^k \frac{\delta\theta}{\delta z} \tag{36}$$

For the k^{th} layer of the shell structure it is supposed that K_1^k, K_2^k, K_3^k are constant because in each layer H_α^k, H_β^k are calculated. For each layer both governing equations and boundary conditions are satisfied by assuming the following temperature field:

$$\theta(\alpha, \beta, z) = f(z)\ \theta_\Omega(\alpha, \beta) \tag{37}$$

where θ_Ω in this paper is considered bi-sinusoidal as follows:

$$\theta_\Omega(\alpha, \beta) = \sin\left(\frac{m\pi\alpha}{a}\right)\sin\left(\frac{n\pi\beta}{b}\right) \tag{38}$$

and $f(z)$ is assumed as:

$$f(z) = \theta_0 \exp\left(s^k z\right) \tag{39}$$

where θ_0 is a constant and s^k a parameter. Substituting 37 in 34 and solving for s^k:

$$s_{1,2}^k = \pm\sqrt{\frac{\frac{K_1^k}{(H_\alpha^k)^2}\left(\frac{m\pi}{a}\right)^2 + \frac{K_2^k}{(H_\beta^k)^2}\left(\frac{n\pi}{b}\right)^2}{K_3^k}} \tag{40}$$

Therefore:

$$f(z) = \theta_{01}^k \exp\left(s_1^k z\right) + \theta_{02}^k \exp\left(s_1^k z\right)$$

or:

$$f(z) = C_1^k \cosh\left(s_1^k z\right) + C_2^k \sinh\left(s_1^k z\right) \tag{41}$$

The solution for a layer k can be written as:

$$\theta_c(\alpha, \beta, z) = \theta^k = \left[C_1^k \cosh\left(s_1^k z\right) + C_2^k \sinh\left(s_1^k z\right)\right] \sin\left(\frac{m\pi\alpha}{a}\right)\sin\left(\frac{n\pi\beta}{b}\right) \tag{42}$$

wherein the coefficients C_1^k and C_2^k are constant for each layer k. In 41 for each layer k two unknowns (C_1^k and C_2^k) remain. Therefore, if the number of layers is N_l, the number of unknowns is $(2\,N_l)$ and $(2\,N_l)$ equations to determine the unknowns are needed. The first two conditions are given by the temperature at the top and the bottom of the shell structure:

$$f(z_{bottom}) = \hat{\theta}_{bottom} = C_1^1 \cosh\left(s_1^1 z_{bottom}\right) + C_2^1 \sinh\left(s_1^1 z_{bottom}\right)$$

$$f(z_{top}) = \hat{\theta}_{top} = C_1^{N_l} \cosh\left(s_1^{N_l} z_{top}\right) + C_2^{N_l} \sinh\left(s_1^{N_l} z_{top}\right) \tag{43}$$

Another $(N_l - 1)$ equations can be obtained from the continuity of temperature at each layer interface as follows:

$$C_1^k \cosh\left(s_1^k z_t^k\right) + C_2^k \sinh\left(s_1^k z_t^k\right) - C_1^{k+1} \cosh\left(s_1^{k+1} z_b^{k+1}\right) - C_2^{k+1} \sinh\left(s_1^{k+1} z_b^{k+1}\right) = 0 \tag{44}$$

and another $(N_l - 1)$ equations can be obtained from the continuity of heat flux through the interfaces as follows:

$$s_1^k K_3^k \left[C_1^k \sinh\left(s_1^k z_t^k\right) + C_2^k \cosh\left(s_1^k z_t^k\right)\right] - s_1^{k+1} K_3^{k+1} \left[C_1^{k+1} \sinh\left(s_1^{k+1} z_b^{k+1}\right) + C_2^{k+1} \cosh\left(s_1^{k+1} z_b^{k+1}\right)\right] = 0 \tag{45}$$

In 44 and 45 subscripts t and b indicate the top and bottom of each layer. Solving the system given by 43, 44 and 45 the $(2\,N_l)$ coefficients C_1^k and C_2^k are obtained. The temperature amplitude in the thickness shell direction is given by:

$$\hat{\theta}_c(z) = \hat{\theta}^k = C_1^k \cosh\left(s_1^k z\right) + C_2^k \sinh\left(s_1^k z\right) \quad \text{for } k = 1, \ldots, N_l \tag{46}$$

So, the explicit expression of the fundamental nucleus $\boldsymbol{\Theta}^{k\tau i}$, is:

$$\Theta_\alpha^{k\tau i} = \lambda_6^k J_\alpha^{k\tau} W_{i,\beta}^k + \lambda_1^k J_\beta^{k\tau} W_{i,\alpha}^k \tag{47}$$

$$\Theta_\beta^{k\tau i} = \lambda_2^k J_\alpha^{k\tau} W_{i,\beta}^k + \lambda_6^k J_\beta^{k\tau} W_{i,\alpha}^k \tag{48}$$

$$\Theta_z^{k\tau i} = \lambda_3^k J_{\alpha\beta}^{k\tau,z} W_i^k + \frac{\lambda_2^k}{R_\beta^k} J_\alpha^{k\tau} W_i^k + \frac{\lambda_1^k}{R_\alpha^k} J_\beta^{k\tau} W_i^k \tag{49}$$

Where the following integrals in the domain Ω_k are defined:

$$\left(W_i^k;\, W_{i,\alpha}^k;\, W_{i,\beta}^k\right) = \int_{\Omega_k} \left(N_i \theta_\Omega;\, \frac{\partial N_i}{\partial \alpha}\theta_\Omega;\, \frac{\partial N_i}{\partial \beta}\theta_\Omega\right) d\alpha_k d\beta_k \tag{50}$$

Moreover, the integrals on the domain A_k, in the thickness direction, are written as:

$$\left(J_\alpha^{k\tau}; J_\beta^{k\tau}; J_{\alpha\beta}^{k\tau,z}\right) = \int_{A_k} \left(F_\tau \hat{\theta}^k H_\alpha^k;\, F_\tau \hat{\theta}^k H_\beta^k;\, \frac{\partial F_\tau}{\partial z}\hat{\theta}^k H_\alpha^k H_\beta^k\right) dz \tag{51}$$

7 Acronyms

Several refined and advanced two-dimensional models are contained in the Unified Formulation. Depending on the variables description (LW, ESL) and the order of expansion N of the displacements in z, a large variety of kinematics shell theories can be obtained. A system of acronyms is given in order to denote these models. The first letter indicates the multi-layer approach which can be Equivalent Single Layer (ESL) or Layer Wise (LW). The number N indicates the order of expansion used in the thickness direction (from 1 to 4). In the case of LW approach, the same order of expansion is used for each layer. In the case of ESL approach, a letter Z can be added if the zig-zag effects of displacements is considered by means of Murakami's zig-zag function. Summarizing, ESL1-ESL4 are ESL models. If Murakami zig-zag function is used, these equivalent single layer models are indicated as ESLZ1-ESLZ3. In the case of layer wise approach, the acronym LW is considered in place of ESL, so the acronyms are LW1-LW4. Sometimes the Navier analytical method is employed in place of the FEM method and a subscript (a) is used. In the case of the calculated temperature profile the solutions are indicated by T_c, while T_a is used for the solutions deriving from an assumed linear temperature profile.

8 Numerical results

This section is composed of two parts. The first one is devoted to the assessment of the shell element based on the Unified Formulation by the static analysis of simply supported plates, cylindrical shells and spherical shells. All of them are evaluated applying a thermal load with a bi-sinusoidal in-plane distribution. Before the assessment results of the static analysis a brief discussion about the evaluation of the temperature profile is given. Using the theory that provides the most accurate results, the second part presents some benchmark solutions relative to plates, cylindrical shells and spherical shells with particular lamination and boundary conditions.

8.1 Temperature profile evaluation

The temperature profile along the thickness direction is given in Figures 5-6 for the plate structure and the cylindrical shell panel, for both the assumed linear profile and the calculated one.

For the three layered composite plate structure (see Figure 5) the calculated profile is plotted for different thickness ratios a/h. It is evident that for thin plates the temperature profile can be assumed almost linear, conversely for thick plates the temperature behavior is very far from the

linear one, and large errors can be committed if the temperature profile is assumed as linear.

For the two layered composite cylindrical shell panel, see Figure 6, the calculated profile is plotted for different thickness to radius ratios R/h and thickness ratio $a/h = 10$. One can note that the effect of the curvature on the distribution of the temperature profile is negligible and the difference with the linear profile is only due to the thickness ratio $a/h = 10$.

The proposed evaluations of temperature profile clarify the importance of a calculated temperature profile for thick plates and shells in order to avoid large errors in the approximation of thermal load.

8.2 Assessment

To assess the efficiency of this shell element, three reference problems are considered: the first one is a cross-ply square multilayered plate with lamination $(0°/90°/0°)$ and simply-supported boundary conditions and is compared with the 3D elasticity solution given by Bhaskar et al. in [43]. The second problem is a square cylindrical panel, analytically analyzed, with lamination $(0°/90°)$ and simply-supported boundary conditions. The last one is a square spherical panel, analytically analyzed, with lamination $(0°/90°)$. The boundary conditions are simply-supported. All of them are analyzed by applying a thermal load with a bi-sinusoidal in-plane distribution:

$$\theta(\alpha, \beta, z) = \hat{\theta}(z) \sin\left(\frac{m\pi\alpha}{a}\right) \sin\left(\frac{n\pi\beta}{b}\right) \qquad (52)$$

where $m = n = 1$. These three problems are briefly described in the following sections.

8.2.1 Multilayered plate

The structure analyzed by Bhaskar et al. [43] (see Figure 3) is a composite multilayered square plate with lamination $(0°/90°/0°)$. The physical properties of the material of the plate, composite, are given in Table 1. The geometrical dimensions are: $a = b = 1\,m$. The temperature boundary conditions are: $\hat{\theta}_{top} = 1\,K$, $\hat{\theta}_{bottom} = -1\,K$. The results are presented for different thickness ratios $a/h = 2, 10, 50, 100$. A mesh grid of 10×10 elements is taken to ensure the convergence of the solution (see Table 2). The values of the transversal displacement w and the transverse shear stress $\sigma_{\alpha z}$ are listed in Table 3 for the temperature profile calculated solving the Fourier heat conduction equation and compared with the assumed linear temperature profile. Other results in terms of transverse shear stress and transversal displacement are shown in Figures 7-10. All the FEM solutions, with an assumed linear temperature profile, lead to accurate results with respect to the $3D$ solution [43], that makes use of the same linear profile assumption. The results agree also with the analytical solutions provided for all the thickness ratios, except in the case of FSDT model. Indeed, plate elements that present a constant transverse normal strain such as $FSDT$ lead to inaccurate results for both thick and thin plates. It is confirmed what found in [12]: at least a parabolic expansion for the displacements (u, v, w) is required to capture the linear thermal strains that are related to a linear through-the-thickness temperature distribution. The results obtained with the calculated temperature profile are close to them of the assumed linear profile for plates with thickness ratios $a/h = 50, 100$, while for plates with thickness ratios $a/h = 2, 10$ the thermal profile is clearly non linear and results are different from the linear cases even if the displacement field is approximated by refined models.

In general, LW theories perform better than ESL ones and generally a lower-order expansion of the displacements is sufficient. Equivalent single layer analyses are quite satisfactory only for the transverse displacement if applied to thin plates $a/h = 100$, but not for the solution of the transverse shear stresses, as shown in Figures 7-10. On the other hand, higher-order LW theories lead to better results but computationally more expensive.

Table 1: Physical data for multilayered plate, cylindrical and spherical shell.

Material	Composite	Carbon
$\frac{E_L}{E_T}$	25.0	25.0
$\frac{G_{LT}}{G_{TT}}$	$\frac{0.5}{0.2}$	$\frac{0.5}{0.2}$
ν	0.25	0.25
$\frac{\alpha_T}{\alpha_L}$	1125.0	3.0
$\frac{K_L}{K_T}$	$\frac{36.42}{0.96}$	$\frac{36.42}{0.96}$

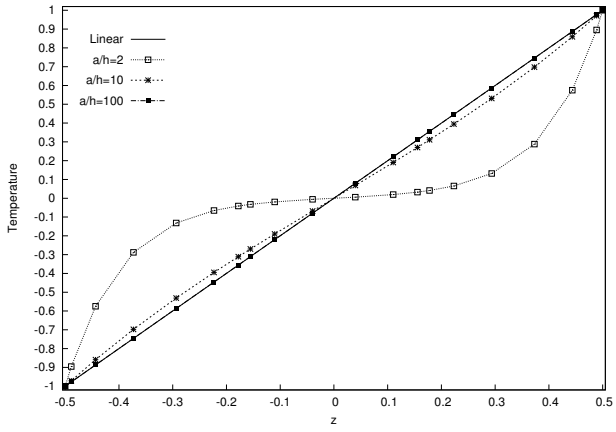

Figure 5: Temperature Profiles for different thickness ratios (a / h). Composite plate.

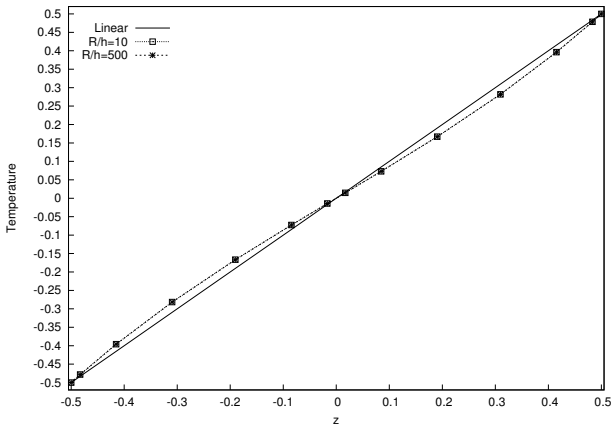

Figure 6: Temperature Profiles for different radius to thickness ratios (R / h). Composite cylinder.

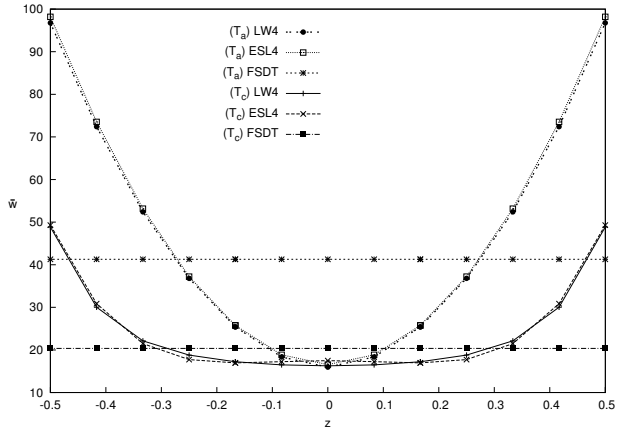

Figure 7: Transverse displacement ***w*** along the thickness, with thickness ratio (a / h) = 2. Composite plate.

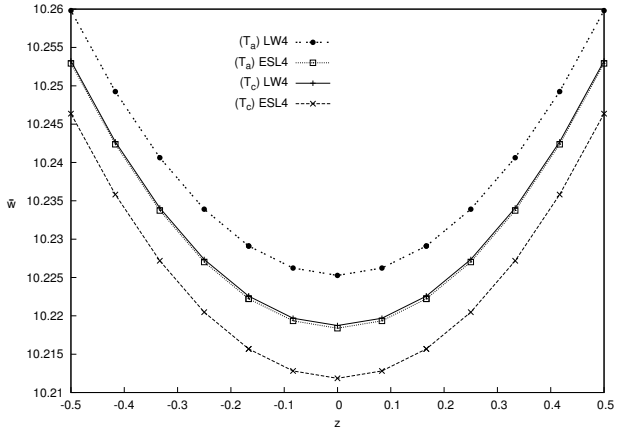

Figure 8: Transverse displacement ***w*** along the thickness, with thickness ratio (a / h) = 100. Composite plate.

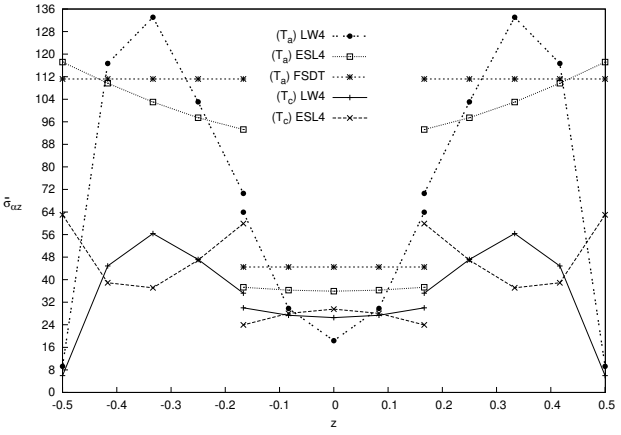

Figure 9: Transverse shear stress $\boldsymbol{\sigma}_{\alpha z}$ along the thickness, with thickness ratio (a / h) = 2. Composite plate.

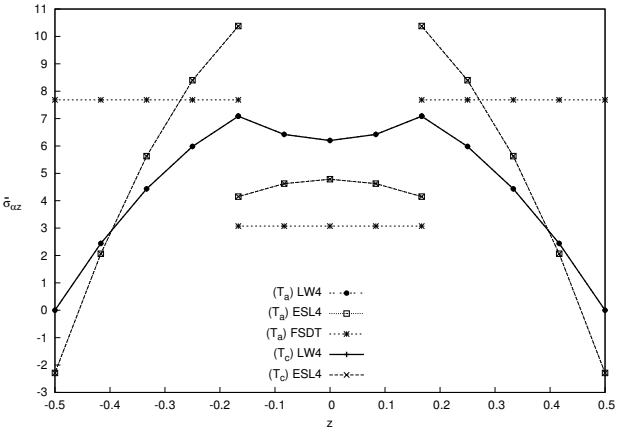

Figure 10: Transverse shear stress $\boldsymbol{\sigma}_{\alpha z}$ along the thickness, with thickness ratio (a / h) = 100. Composite plate.

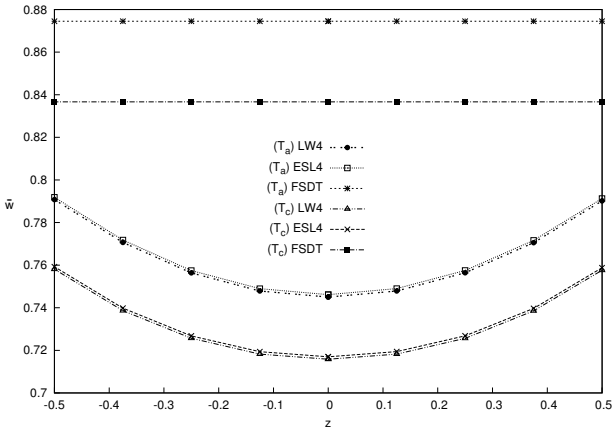

Figure 11: Transverse displacement ***w*** along the thickness, with radius to thickness ratio (R / h) = 10. Composite cylindrical panel.

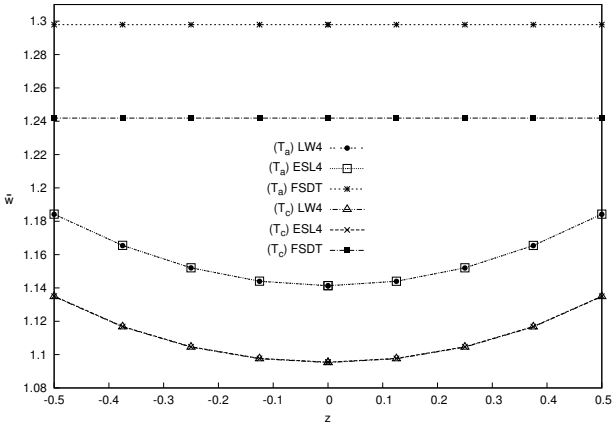

Figure 12: Transverse displacement ***w*** along the thickness, with radius to thickness ratio (R / h) = 500. Composite cylindrical panel.

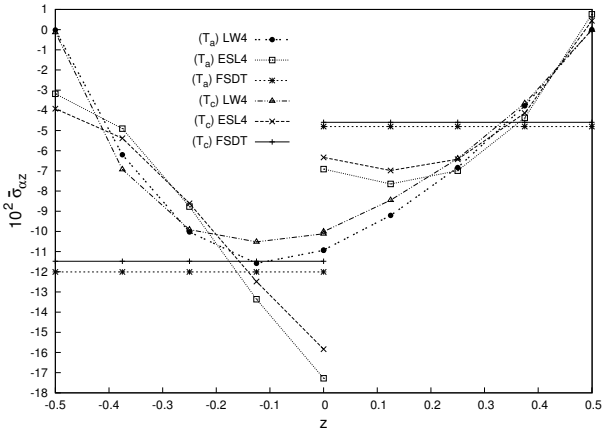

Figure 13: Transverse shear stress $\sigma_{\alpha z}$ along the thickness, with radius to thickness ratio (R / h) = 10. Composite cylindrical panel.

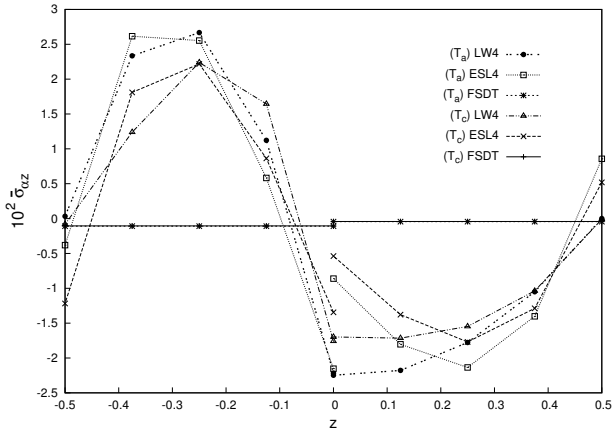

Figure 14: Transverse shear stress $\sigma_{\alpha z}$ along the thickness, with radius to thickness ratio (R / h) = 500. Composite cylindrical panel.

Table 2: Convergence study. Plate with thickness ratio a/h = 100, cylindrical panel and spherical panel with radius to thickness ratio R/h = 500. All the cases are computed for the calculated temperature profile T_c and with a $LW4$ theory.

	Mesh	4 × 4	6 × 6	8 × 8	10 × 10	*Analytical*
Plate	w	10.27	10.26	10.25	10.25	10.25
	σ_{xz}	7.466	7.213	7.102	7.084	7.069
Cylindrical	w	1.0966	1.0955	1.0953	1.0952	1.0953
	$\sigma_{\alpha z}$	-1.7090	-1.7131	-1.7093	-1.6983	-1.6957
Spherical	w	1.0958	1.0948	1.0946	1.0945	1.0945
	$\sigma_{\alpha z}$	-2.2848	-2.2065	-2.1562	-2.1461	-2.1403

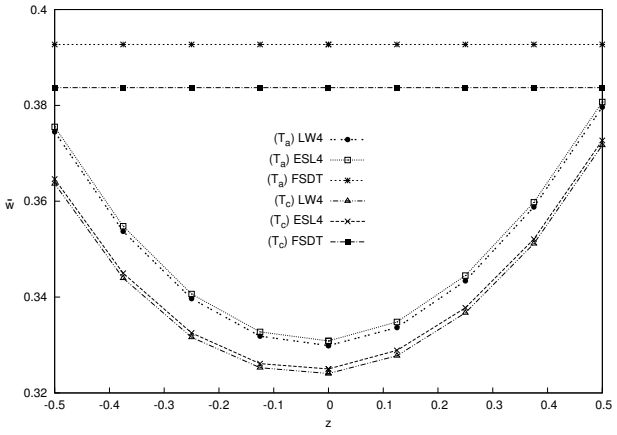

Figure 15: Transverse displacement $\boldsymbol{w}$ along the thickness, with radius to thickness ratio (R / h) = 10. Composite spherical panel.

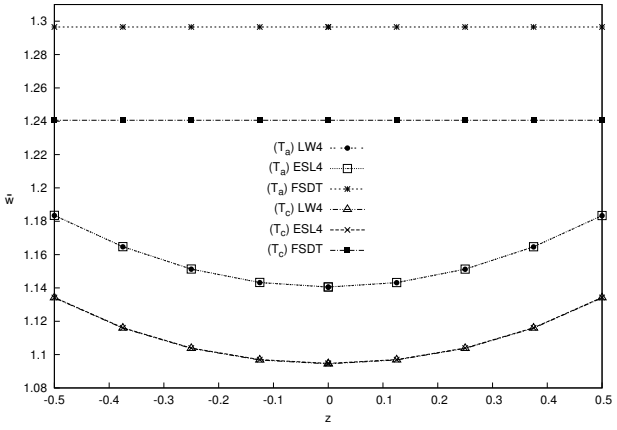

Figure 16: Transverse displacement $\boldsymbol{w}$ along the thickness, with radius to thickness ratio (R / h) = 500. Composite spherical panel.

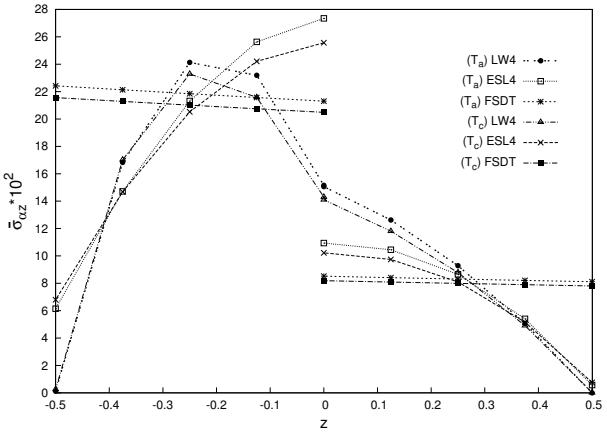

Figure 17: Transverse shear stress $\boldsymbol{\sigma}_{\alpha z}$ along the thickness, with radius to thickness ratio (R / h) = 10. Composite spherical panel.

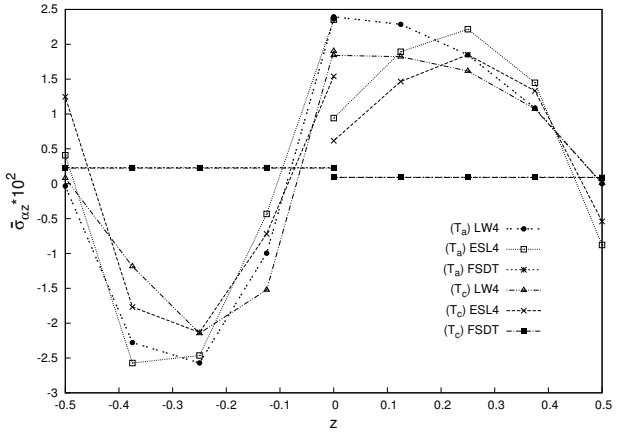

Figure 18: Transverse shear stress $\boldsymbol{\sigma}_{\alpha z}$ along the thickness, with radius to thickness ratio (R / h) = 500. Composite spherical panel.

8.2.2 Multilayered cylindrical panel

In this section, a cylindrical composite panel with lamination (0°/90°) is analyzed (see Figure 2). The lamination angle is 0° for the bottom layer and 90° for the top layer. The geometrical dimensions are: a = 1 m and b = 1 m, global thickness h_{tot} = 0.1 m, curvature radius $R_\alpha = \infty$. The physical properties of the carbon are given in Table 1. The temperature boundary conditions are: $\hat{\theta}_{top}$ = 0.5 K, $\hat{\theta}_{bottom}$ = −0.5 K for all the cases. The results are compared with the corresponding closed form solutions obtained with the Navier method and are presented for different radius to thickness ratios R_β/h_{tot} = 10 , 50 , 100 , 500 with the corresponding curvature radii R_β = 1 , 5 , 10 , 50. A mesh grid of 10 × 10 elements is taken to ensure the convergence of the solution (see Table 2). The values of the transversal displacement w and the transverse shear stress $\sigma_{\alpha z}$ are listed in Table 4 for the temperature profile calculated solving the Fourier's heat conduction equation and compared with the assumed linear temperature profile. Other results in terms of transverse shear stress and transversal displacement are shown in Figures 11-14.

All the FEs, in both calculated and assumed linear cases, lead to accurate results with respect to the analytical solutions for all the thickness ratios, except for FSDT elements. The difference between the calculated temperature profile and the assumed linear one is a constant and it is not affected by the curvature of the cylinder R_β; this difference is due to the thickness ratio which is a/h = 10. In general, LW theories perform better than ESL ones and often also with a lower-order expansion of the unknowns. Equivalent single layer analyses are quite satisfactory for the transverse displacement, even when lower radii to thick-

Table 3: Plate with lamination $(0°/90°/0°)$. Transverse displacement $w = w(a/2, b/2) * h_{tot}$, evaluated at $z = \pm h/2$. Transverse shear stress $\sigma_{xz} = \sigma_{xz}(a, 0)$, evaluated at $z = +h/6$.

	a/h		2	10	50	100
w	$3D$[43]		96.79	17.39	10.50	10.26
σ_{xz}	$3D$[43]		63.92	60.54	14.07	7.073
w	$LW4_a$	T_a	96.78	17.39	10.50	10.26
		T_c	49.09	16.39	10.47	10.25
	$LW4$	T_a	96.77	17.39	10.50	10.26
		T_c	48.85	16.39	10.47	10.25
	$LW1$	T_a	89.23	17.62	11.14	10.91
		T_c	44.17	16.69	11.11	10.91
	$ESLZ3$	T_a	94.85	17.37	10.50	10.26
		T_c	50.08	16.41	10.47	10.25
	$ESL4_a$	T_a	98.21	16.90	10.47	10.25
		T_c	49.55	15.93	10.44	10.25
	$ESL4$	T_a	98.20	16.90	10.47	10.25
		T_c	49.29	15.93	10.44	10.25
	$ESL2$	T_a	83.45	14.96	10.38	10.23
		T_c	40.87	14.09	10.35	10.22
	$FSDT$	T_a	41.27	18.33	15.17	15.06
		T_c	20.35	17.26	15.13	15.05
σ_{xz}	$LW4_a$	T_a	63.82	60.54	14.07	7.073
		T_c	30.11	57.07	14.04	7.069
	$LW4$	T_a	63.93	60.66	14.10	7.088
		T_c	30.00	57.18	14.07	7.084
	$LW1$	T_a	42.54	58.78	13.69	6.883
		T_c	31.69	56.35	13.21	6.879
	$ESLZ3$	T_a	27.42	52.61	12.45	6.263
		T_c	23.42	50.43	12.43	6.260
	$ESL4_a$	T_a	37.25	36.33	8.251	4.143
		T_c	24.04	34.47	8.232	4.140
	$ESL4$	T_a	37.30	36.41	8.268	4.152
		T_c	23.96	34.55	8.250	4.149
	$ESL2$	T_a	11.58	16.21	3.624	1.819
		T_c	6.065	15.31	3.616	1.818
	$FSDT$	T_a	44.48	28.00	6.127	3.073
		T_c	22.09	26.41	6.112	3.071

ness ratios are considered ($R/h = 10$), but not for the transverse shear stress, as shown in Figures 11-14.

Table 4: Cylindrical panel with lamination $(0°/90°)$. Transverse displacement $w = w(a/2, b/2)$, transverse shear stress $\sigma_{\alpha z} = \sigma_{\alpha z}(a, 0) * 10^2$, evaluated at $z = 0$.

	R_β/h		10	50	100	500
w	$LW4_a$	T_a	0.7450	1.1192	1.1359	1.1412
		T_c	0.7188	1.0748	1.0904	1.0953
	$LW4$	T_a	0.7450	1.1192	1.1359	1.1412
		T_c	0.7158	1.0743	1.0902	1.0952
	$LW1$	T_a	0.7712	1.1538	1.1706	1.1759
		T_c	0.7412	1.1082	1.1243	1.1293
	$ESLZ3$	T_a	0.7454	1.1177	1.1342	1.1396
		T_c	0.7147	1.0717	1.0875	1.0926
	$ESL4_a$	T_a	0.7461	1.1194	1.1360	1.1413
		T_c	0.7199	1.0751	1.0907	1.0955
	$ESL4$	T_a	0.7461	1.1194	1.1360	1.1413
		T_c	0.7170	1.0746	1.0904	1.0955
	$ESL2$	T_a	0.7455	1.1152	1.1316	1.1369
		T_c	0.7150	1.0695	1.0852	1.0902
	$FSDT$	T_a	0.8745	1.2781	1.2941	1.2979
		T_c	0.8367	1.2229	1.2382	1.2419
$\sigma_{\alpha z}$	$LW4_a$	T_a	−10.901	−3.7541	−2.8789	−2.2428
		T_c	−10.051	−3.1516	−2.3086	−1.6957
	$LW4$	T_a	−10.923	−3.7615	−2.8845	−2.2471
		T_c	−10.011	−3.1485	−2.3086	−1.6983
	$LW1$	T_a	−8.3115	−4.0011	−3.5188	−3.1781
		T_c	−7.7544	−3.6140	−3.1507	−2.8235
	$ESLZ3$	T_a	−10.522	−3.5686	−2.7832	−2.2277
		T_c	−9.7816	−3.1176	−2.3651	−1.8329
	$ESL4_a$	T_a	−6.8978	−1.7276	−1.2097	−0.8599
		T_c	−6.3568	−1.3735	−0.8747	−0.5374
	$ESL4$	T_a	−6.9120	−1.7309	−1.2120	−0.8614
		T_c	−6.3345	−1.3701	−0.8732	−0.5377
	$ESL2$	T_a	−5.6195	−1.7814	−1.4294	−1.2006
		T_c	−5.3090	−1.6296	−1.2921	−1.0727
	$FSDT$	T_a	−4.8037	−0.6032	−0.2571	−0.0436
		T_c	−4.5916	−0.5767	−0.2457	−0.0418

Table 5: Spherical panel with lamination $(0°/90°)$. Transverse displacement $w = w(a/2, b/2)$, evaluated at $z = 0$, transverse shear stress $\sigma_{\alpha z} = \sigma_{\alpha z}(a, 0) * 10^2$ evaluated at $z = -h/4$.

	R/h		10	50	100	500
w	$LW4_a$	T_a	0.3299	1.0507	1.1174	1.1404
		T_c	0.3203	1.0087	1.0725	1.0945
	$LW4$	T_a	0.3299	1.0507	1.1174	1.1405
		T_c	0.3240	1.0091	1.0726	1.0945
	$LW1$	T_a	0.3386	1.0836	1.1516	1.1751
		T_c	0.3325	1.0414	1.1062	1.1285
	$ESLZ3$	T_a	0.3306	1.0496	1.1159	1.1388
		T_c	0.3235	1.0071	1.0701	1.0918
	$ESL4_a$	T_a	0.3309	1.0511	1.1176	1.1406
		T_c	0.3213	1.0093	1.0728	1.0947
	$ESL4$	T_a	0.3309	1.0511	1.1176	1.1406
		T_c	0.3250	1.0096	1.0729	1.0947
	$ESL2$	T_a	0.3315	1.0477	1.1134	1.1361
		T_c	0.3248	1.0054	1.0679	1.0895
	$FSDT$	T_a	0.3927	1.1967	1.2709	1.2965
		T_c	0.3837	1.1459	1.2163	1.2406
$\sigma_{\alpha z}$	$LW4_a$	T_a	24.096	1.1199	-1.3854	-2.5674
		T_c	23.379	1.3972	-1.0041	-2.1403
	$LW4$	T_a	24.131	1.1212	-1.3877	-2.5714
		T_c	23.289	1.3831	-1.0122	-2.1461
	$LW1$	T_a	19.500	1.5598	-0.5309	-1.5931
		T_c	18.818	1.6718	-0.3315	-1.3536
	$ESLZ3$	T_a	21.061	2.4154	0.1275	-1.0771
		T_c	20.328	2.5096	0.3181	-0.8407
	$ESL4_a$	T_a	21.281	0.8662	-1.3842	-2.4603
		T_c	20.593	1.0635	-1.0932	-2.1270
	$ESL4$	T_a	21.312	0.8673	-1.3865	-2.4641
		T_c	20.521	1.0521	-1.1000	-2.1325
	$ESL2$	T_a	20.284	3.0723	0.9925	-0.0983
		T_c	19.598	3.1406	1.1473	0.0970
	$FSDT$	T_a	21.845	3.9515	1.5581	0.2307
		T_c	21.011	3.8024	1.5047	0.2240

Table 6: Benchmark problems. Case 1 with anti-simmetric lamination ±45°. Plate, cylindrical and spherical panel, transverse displacement $w = 10\, w(a/2, b/2, +h/2)$ and transverse shear stress $\sigma_{\alpha z} = 10^2\, \sigma_{\alpha z}(a, b/2, 0)$.

			Plate		*Cylindrical*			*Spherical*	
	a/h		10	100	R/h	10	100	10	100
w	*LW4*	T_a	1375.4	4607.8		4.8796	7.4058	2.6295	7.4971
		T_c	1293.5	4604.7		4.5741	7.0165	2.5533	7.1029
	LW1	T_a	1274.3	4895.2		4.7358	7.5077	2.4930	7.6005
		T_c	1203.2	4892.2		4.4477	7.1343	2.4305	7.2202
	ESLZ3	T_a	1307.7	4586.4		4.7120	7.3351	2.5257	7.4200
		T_c	1232.7	4583.4		4.4154	6.9528	2.4542	7.0325
	ESL4	T_a	1250.8	4550.1		4.7274	7.3978	2.5388	7.4776
		T_c	1177.8	4547.1		4.4239	7.0045	2.4615	7.0793
	ESL2	T_a	1164.1	4501.7		4.7187	7.2171	2.5756	7.3229
		T_c	1096.3	4498.8		4.4192	6.8330	2.5029	6.9316
	FSDT	T_a	1294.9	7222.5		5.0729	7.5539	2.6941	7.6548
		T_c	1219.4	7217.9		4.8079	7.2151	2.6483	7.3099
$\sigma_{\alpha z}$	*LW4*	T_a	-85.932	-56.181		15.624	2.4665	24.592	3.7828
		T_c	-81.708	-56.148		14.483	1.9577	22.964	3.2169
	LW1	T_a	-98.335	-56.066		17.223	5.5156	23.450	6.7916
		T_c	-93.436	-56.033		16.299	5.1621	22.161	6.3780
	ESLZ3	T_a	-97.289	-55.800		17.350	2.6837	26.823	4.0857
		T_c	-92.420	-55.767		16.512	2.5503	25.369	3.8853
	ESL4	T_a	-80.357	-52.295		16.651	0.3544	27.067	1.8573
		T_c	-76.298	-52.264		15.711	0.2248	25.347	1.6474
	ESL2	T_a	-61.532	-37.094		15.936	2.8891	23.900	4.2028
		T_c	-58.089	-37.072		15.343	2.9668	22.689	4.2054
	FSDT	T_a	-92.857	-45.626		12.861	2.2035	20.014	3.2885
		T_c	-87.595	-45.598		12.219	2.0645	18.994	3.0974

8.2.3 Multilayered spherical panel

In this section, a square, spherical panel is analysed (see Figure 1). The temperature boundary conditions are: $\hat{\theta}_{top} = 0.5$ K, $\hat{\theta}_{bottom} = -0.5$ K for all the cases. The results are compared with the analytical solutions obtained with the Navier method. A mesh grid of 10×10 elements is taken to ensure the convergence of the solution (see Table 2). The geometrical dimensions are: $a = 1$ m and $b = 1$ m, global thickness $h_{tot} = 0.1$ m and curvature radii $R_\alpha = R_\beta = R$. The physical properties of the carbon are given in Table 1. The results are presented for different radius to thickness ratios $R/h_{tot} = 10\,,\ 50\,,\ 100\,,\ 500$ with the corresponding curvature radius $R = 1.0\,,\ 5.0\,,\ 10.0\,,\ 50.0$). The lamination angle is 0° for the bottom layer and 90° for the top layer. The values of the transversal displacement w and the transverse shear stress $\sigma_{\alpha z}$ are listed in Table 5 for the temperature profile calculated solving the Fourier heat conduction equation and compared with the assumed linear temperature profile. Other results in terms of transverse shear stress and transversal displacement are shown in Figures 15-18.

Considerations similar to the previous problem can be made. All the FEs, in both calculated and assumed linear cases, lead to accurate results with respect to the analytical solutions for all the thickness ratios, except for FSDT

Table 7: Benchmark problems. Case 2 with clamped-free boundary condition. Plate, cylindrical and spherical panel, transverse displacement $w = 10\, w(a/2, b/2, +h/2)$ and transverse shear stress $\sigma_{\alpha z} = 10^2\, \sigma_{\alpha z}(a, b/2, 0)$.

			Plate			*Cylindrical*		*Spherical*	
	a/h		10	100	R/h	10	100	10	100
w	$LW4$	T_a	1226.8	3096.9		4.5476	5.3307	-0.3479	3.7373
		T_c	1157.7	3094.9		4.3447	5.1018	-0.1750	3.6265
	$LW1$	T_a	1210.9	3274.4		4.6164	5.3874	-0.3642	3.8575
		T_c	1145.2	3272.3		4.4100	5.1571	-0.1923	3.7404
	$ESLZ3$	T_a	1222.0	3096.8		4.5239	5.2945	-0.3407	3.7334
		T_c	1155.2	3094.9		4.3237	5.0705	-0.1681	3.6250
	$ESL4$	T_a	1183.3	3083.9		4.5479	5.3215	-0.3423	3.7477
		T_c	1116.2	3081.9		4.3460	5.0941	-0.1696	3.6368
	$ESL2$	T_a	986.40	3048.6		4.5152	5.2473	-0.3369	3.7263
		T_c	929.51	3046.7		4.3093	5.0195	-0.1652	3.6119
	$FSDT$	T_a	1039.7	4356.4		4.7747	5.5564	-0.5836	3.9916
		T_c	979.72	4353.6		4.5553	5.3129	-0.4107	3.8624
$\sigma_{\alpha z}$	$LW4$	T_a	-2619.8	-522.26		-3.9875	-5.1179	15.086	0.2373
		T_c	-2519.9	-522.01		-3.9154	-5.0207	13.754	-0.0535
	$LW1$	T_a	-2655.5	-579.97		-1.5318	-2.3709	14.765	1.8361
		T_c	-2520.6	-579.67		-1.5150	-2.3397	13.594	1.5630
	$ESLZ3$	T_a	-2436.3	-537.18		-2.9825	-3.9052	14.614	0.8821
		T_c	-2303.2	-536.90		-2.8354	-3.7432	13.481	0.6988
	$ESL4$	T_a	-2695.3	-465.54		-3.3266	-4.2840	14.134	0.4614
		T_c	-2582.7	-465.30		-3.2708	-4.2082	12.905	0.1929
	$ESL2$	T_a	-2287.1	-240.08		-2.8190	-3.6334	13.936	0.7940
		T_c	-2159.2	-239.94		-2.7079	-3.5120	12.809	0.5937
	$FSDT$	T_a	-4195.5	-446.19		-6.0953	-6.9657	13.570	-2.0926
		T_c	-3955.6	-445.91		-5.7896	-6.6468	12.506	-2.1219

elements. The difference between the calculated temperature profile solutions and the assumed linear one is constant and it is not affected by the curvature R_β. In general, LW theories perform better than ESL ones and generally a lower-order expansion of the unknowns is sufficient. Equivalent single layer analyses are quite satisfactory only for the transverse displacement, even for lower radii to thickness ratios ($R/h = 10$). Figures 15-18 show a different behavior for the transverse shear stress, where higher-order LW models are required to get accurate results.

8.3 FEM benchmark solutions

Similar plates, cylindrical shells and spherical shells are analyzed, considering two new problems that have not reference analytical solutions:

1. Structures with lamination $\pm 45^\circ$ under bi-sinusoidal load and simply-supported boundary conditions.
2. Structures with clamped-free boundary conditions: edges parallel to β-direction clamped and those parallel to α-direction free. The lamination is equal to the assessment cases.

8.3.1 Anti-simmetric lamination ±45°

The first structure analyzed is a composite multilayered square plate with lamination (−45°/45°/−45°). The physical properties of the material, the geometrical data and the temperature boundary conditions are the same of the assessment cases. The structure is simply supported. The results are presented for different thickness ratios a/h = 10, 100. The same mesh grid of 10 × 10 elements of the assessment cases is taken to ensure the convergence of the solution. The values of the transversal displacement w and the transverse shear stress $\sigma_{\alpha z}$ are listed in Table 6.

The second structure analyzed is a composite square cylindrical panel with lamination (−45°/45°). The lamination angle is −45° for the bottom layer and 45° for the top layer. The physical properties of the material, the geometrical data and the temperature boundary conditions are the same of the assessment cases. The structure is simply supported. The results are presented for different radius to thickness ratios R/h = 10, 100. The same mesh grid of 10 × 10 elements of the assessment cases is taken to ensure the convergence of the solution. The values of the transversal displacement w and the transverse shear stress $\sigma_{\alpha z}$ are listed in Table 6.

The last structure analyzed is a composite square spherical panel with lamination (−45°/45°). The lamination angle is −45° for the bottom layer and 45° for the top layer. The physical properties of the material, the geometrical data and the temperature boundary conditions are the same of the assessment cases. The structure is simply supported. The results are presented for different radius to thickness ratios R/h = 10, 100. The same mesh grid of 10×10 elements of the assessment cases is taken to ensure the convergence of the solution. The values of the transversal displacement w and the transverse shear stress $\sigma_{\alpha z}$ are listed in Table 6.

8.3.2 Clamped-free boundary conditions

In this part, the structures are considered with clamped-free boundary conditions: edges parallel to β-direction clamped and those parallel to α-direction free.
The first structure analyzed is a composite multilayered square plate. The physical properties of the material, the lamination angle, the geometrical data and the temperature boundary conditions are the same of the assessment cases. The results are presented for different thickness ratios a/h = 10, 100. The same mesh grid of 10×10 elements of the assessment cases is taken to ensure the convergence of the solution. The values of the transversal displacement w and the transverse shear stress $\sigma_{\alpha z}$ are listed in Table 7.

The second structure analyzed is a composite square cylindrical panel. The physical properties of the material, the lamination angle, the geometrical data and the temperature boundary conditions are the same of the assessment cases. The results are presented for different radius to thickness ratios R/h = 10, 100. The same mesh grid of 10×10 elements of the assessment cases is taken to ensure the convergence of the solution. The values of the transversal displacement w and the transverse shear stress $\sigma_{\alpha z}$ are listed in Table 7.

The last structure analyzed is a composite square spherical panel. The physical properties of the material, the lamination angle, the geometrical data and the temperature boundary conditions are the same of the assessment cases. The results are presented for different radius to thickness ratios R/h = 10, 100. The same mesh grid of 10×10 elements of the assessment cases is taken to ensure the convergence of the solution. The values of the transversal displacement w and the transverse shear stress $\sigma_{\alpha z}$ are listed in Table 7.

9 Conclusions

This paper has dealt with the static analysis of composite shells by means of a finite element based on the Unified Formulation by Carrera. An assessment of the element has been performed by analyzing simply-supported cross-ply plates, cylindrical and spherical shells under bi-sinusoidal thermal load with both calculated thermal profile (solving the Fourier heat conduction equation) and assumed linear temperature profile. The results have been presented in terms of both transversal displacements and transverse shear stresses, for various thickness ratios and curvature ratios. The performances of the shell element have been tested, and the different theories (classical and refined) contained in the CUF have been compared. The conclusions that can be drawn are the following:

1. The shell element is locking free, for all the LW and ESL models considered. The results converge to the reference solution by increasing both the mesh and the order of expansion of the displacements in the thickness direction.
2. LW models work better than ESLZ theories, and these last perform better than ESL models in thick shell cases.

3. The classical models, such as FSDT, lead to erroneous results in the analysis of thermal problem, even in the case of thin shells.
4. The use of LW models produces better results for both thick and thin shells. Their use becomes mandatory if an accurate description of transverse stresses along the thickness and fulfillment of interlaminar continuity conditions are required.

Finally, some benchmark solutions have been calculated for plates, cylindrical and spherical shells that have not analytical reference solutions: lamination $(-45°/45°)$ and clamped-free boundary conditions have been considered. The results have been presented in terms of transversal displacement and transverse shear stresses in the form of tables.

References

[1] T. Kant, R. K. Khare, Finite element thermal stress analysis of composite laminates using a higher-order theory, Journal of Thermal Stresses, 17(2) ()1994, 229–255.

[2] A. A. Khdeir, J. N. Reddy, Thermal stresses and deflections of cross-ply laminated plates using refined plate theories, Journal of Thermal Stresses, 14(4) (1991), 419–438.

[3] W. Zhen, C. Wanji, A global-local higher order theory for multilayered shells and the analysis of laminated cylindrical shell panels, Composite Structures, 84(4) (2008), 350–361.

[4] R. K. Khare, T. Kant, A. .K Garg, Closed-form thermo-mechanical solutions of higher-order theories of cross-ply laminated shallow shells, Composite Structures, 59(3) (2003), 313–340.

[5] A. A. Khdeir, Thermoelastic analysis of cross-ply laminated circular cylindrical shells, International Journal of Solids and Structures, 33(27) (1996), 4007–4017.

[6] A. A. Khdeir, M. D. Rajab, J. N. Reddy, Thermal effects on the response of cross-ply laminated shallow shells, International Journal of Solids and Structures, 29(5) (1992), 653–667.

[7] A. Barut, E. Madenci, A. Tessler, Nonlinear thermoelastic analysis of composite panels under non-uniform temperature distribution, International Journal of Solids and Structures, 37(27) (2000), 3681–3713.

[8] C. J. Miller, W. A. Millavec, T. P. Richer, Thermal stress analysis of layered cylindrical shells, AIAA Journal, 19(4) (1981), 523–530.

[9] P. C. Dumir, J. K. Nath, P. Kumari, S. Kapuria, Improved efficient zigzag and third order theories for circular cylindrical shells under thermal loading, Journal of Thermal Stresses, 31(4) (2008), 343–367.

[10] Y. S. Hsu, J. N. Reddy, C. W. Bert, Thermoelasticity of circular cylindrical shells laminated of bimodulus composite materials, Journal of Thermal Stresses, 4(2) (1981), 155–177.

[11] K. Ding, Thermal stresses of weak formulation study for thick open laminated shell, Journal of Thermal Stresses, 31(4) (2008), 389–400.

[12] E. Carrera, Temperature profile influence on layered plates response considering classical and advanced theories, AIAA Journal, 40(9) (2002), 1885–1896.

[13] E. Carrera, An assessment of mixed and classical theories for the thermal stress analysis of orthotropic multilayered plates, Journal of Thermal Stresses, 23(9) (2000), 797–831.

[14] A. Robaldo, E. Carrera, Mixed finite elements for thermoelastic analysis of multilayered anisotropic plates, Journal of Thermal Stresses, 30 (2007), 165–194.

[15] P. Nali, E. Carrera, A. Calvi, Advanced fully coupled thermo-mechanical plate elements for multilayered structures subjected to mechanical and thermal loading, International Journal for Numerical Methods in Engineering, 85 (2011), 869–919.

[16] E. Carrera, A. Ciuffreda, Closed-form solutions to assess multilayered-plate theories for various thermal stress problems, Journal of Thermal Stresses, 27 (2004), 1001–1031.

[17] E. Carrera, M. Cinefra, F. A. Fazzolari, Some results on thermal stress of layered plates and shells by using Unified Formulation, Journal of Thermal Stresses, 36 (2013), 589–625.

[18] S. Brischetto, R. Leetsch, E. Carrera, T. Wallmersperger, B. Kröplin, Thermo-mechanical bending of functionally graded plates, Journal of Thermal Stresses, 31(3) (2008), 286–308.

[19] F. A. Fazzolari, E. Carrera, Thermal stability of FGM sandwich plates under various through-the-thickness temperature distributions, Journal of Thermal Stresses, 37 (2014), 1449–1481.

[20] S. Brischetto, E. Carrera, Thermal stress analysis by refined multilayered composite shell theories, Journal of Thermal Stresses, 32(1-2) (2009), 165–186.

[21] S. Brischetto, E. Carrera, Heat conduction and thermal analysis in multilayered plates and shells, Mechanics Research Communications, 38 (2011), 449–455.

[22] M. Cinefra, E. Carrera, S. Brischetto, S. Belouettar, Thermo-mechanical analysis of functionally graded shells, Journal of Thermal Stresses, 33 (2010), 942–963.

[23] A. Robaldo, E. Carrera, A. Benjeddou, Unified formulation for finite element thermoelastic analysis of multilayered anisotropic composite plates, Journal of Thermal Stresses, 28 (2005), 1031–1065.

[24] E. Carrera, Theories and finite elements for multilayered, anisotropic, composite plates and shells, Archives of Computational Methods in Engineering, 9(2) (2002), 87–140.

[25] E. Carrera, Theories and finite elements for multilayered plates and shells: a unified compact formulation with numerical assessment and benchmarking, Archives of Computational Methods in Engineering, 10(3) (2003), 215–296.

[26] K. J. Bathe, P. S. Lee, J. F. Hiller, Towards improving the MITC9 shell element, Computers and Structures, 81 (2003), 477–489.

[27] C. Chinosi, L. Della Croce, Mixed-interpolated elements for thin shell, Communications in Numerical Methods in Engineering, 14 (1998), 1155–1170.

[28] N. C. Huang, Membrane locking and assumed strain shell elements, Computers and Structures, 27(5) (1987), 671–677.

[29] P. Panasz, K. Wisniewski, Nine-node shell elements with 6 dofs/node based on two-level approximations. Part I theory and linear tests, Finite Elements in Analysis and Design, 44 (2008), 784–796.

[30] A. W. Leissa, Vibration of shells, NASA National Aeronautics and Space Administration, Washington, DC, SP-288, 1973.

[31] E. Carrera, Multilayered shell theories accounting for layerwise mixed description, Part 1: governing equations, AIAA Journal, 37(9) (1999), 1107–1116.

[32] E. Carrera, Multilayered shell theories accounting for layerwise mixed description, Part 2: numerical evaluations, AIAA Journal, 37(9) (1999), 1117–1124.

[33] W. T. Koiter, On the foundations of the linear theory of thin elastic shell, Proc. Kon. Nederl. Akad. Wetensch., 73 (1970), 169–195.

[34] P. G. Ciarlet, L. Gratie, Another approach to linear shell theory and a new proof of Korn's inequality on a surface, C. R. Acad. Sci. Paris, I,340 (2005), 471–478.

[35] P. M. Naghdi, The theory of shells and plates, Handbuch der Physic, 4 (1972), 425–640.

[36] M. Cinefra, E. Carrera, S. Valvano, Variable Kinematic Shell Elements for the Analysis of Electro-Mechanical Problems, Mechanics of Advanced Materials and Structures, 22(1-2) (2015), 77–106.

[37] H. Murakami, Laminated composite plate theory with improved in-plane responses, Journal of Applied Mechanics, 53 (1986), 661–666.

[38] J.N. Reddy, Mechanics of Laminated Composite Plates, Theory and Analysis, Journal of Applied Mechanics, CRC Press, 1997.

[39] K. J. Bathe, E. Dvorkin, A formulation of general shell elements - the use of mixed interpolation of tensorial components, International Journal for Numerical Methods in Engineering, 22 (1986), 697–722.

[40] M. L. Bucalem, E. Dvorkin, Higher-order MITC general shell elements. International Journal for Numerical Methods in Engineering, 36 (1993), 3729–3754.

[41] M. Cinefra, S. Valvano, A variable kinematic doubly-curved MITC9 shell element for the analysis of laminated composites, Mechanics of Advanced Materials and Structures, (in press).

[42] V. Tungikar, B. K. M. Rao, Three dimensional exact solution of thermal stresses in rectangular composite laminates, Composite Structures, 27(4) (1994), 419–430.

[43] K. Bhaskar, T. K. Varadan, J. S. M. Ali, Thermoelastic solutions for orthotropic and anisotropic composite laminates, Composites: Part B, 27(B) (1996), 415–420.

[44] T. J. R. Hughes, M. Cohen, M. Horaun, Reduced and selective integration techniques in the finite element methods, Nuclear Engineering and Design, 46 (1978), 203–222.